Atropisomerism in Triarylboranes

Doan, Thu Hong; Chardon, Aurelien; Vanthuyne, Nicolas; Ramos, Tárcius N.; Tumanov, Nikolay; Fusaro, Lucas; Albalat, Muriel; Collard, Laurent; Wouters, Johan; Champagne, Benoît; Berionni, Guillaume

Published in:
Angewandte Chemie. International edition

DOI:
10.1002/anie.202421931

Publication date:
2025

Document Version
Publisher's PDF, also known as Version of record

How to cite: *Angew. Chem. Int. Ed.* **2025**, e202421931
doi.org/10.1002/anie.202421931

Atropisomerism

Atropisomerism in Triarylboranes: Lewis Base Assisted Rotation at C–B Stereogenic Axis in Asymmetrical Boron Lewis Acids

Thu-Hong Doan, Aurélien Chardon, Nicolas Vanthuyne, Tárcius N. Ramos, Nikolay Tumanov, Luca Fusaro, Muriel Albalat, Laurent Collard, Johan Wouters, Benoît Champagne, and Guillaume Berionni**

Abstract: The synthesis, properties and structural requirements for atropisomerism at the C–B bond in boron Lewis acids such as triarylboranes have been understudied so far. We report the first series of atropisomeric triarylboranes constituted of a naphthyl rotor and a dihydro-9-bora-anthracenyl stator subunits, connected by a C–B stereogenic axis. Through systematic crystallographic, kinetic, photophysical and quantum chemical studies, the mechanisms, rates and barriers of diastereomerization and enantiomerization were determined. The orthogonal arrangement between the naphthyl and the dihydro-9-bora-anthracenyl scaffold moiety hamper the rotation of these two moieties around their Csp^2–B bonds, enabling chiral resolution leading to enantiopure triarylboranes of high configurational stability. Furthermore, we fully elucidated a Lewis-base assisted pathway controlling the rotation speed at the C–B stereogenic axis, enabling the atropisomerical behavior of these triarylboranes be controlled by a Lewis base.

[*] Dr. T.-H. Doan, Dr. A. Chardon, Dr. T. N. Ramos, Dr. N. Tumanov, Dr. L. Fusaro, Prof. J. Wouters, Prof. B. Champagne, Prof. G. Berionni
Department of Chemistry, NISM Research Institute
University of Namur – 61 Rue de Bruxelles, 5000 Namur, Belgium
E-mail: thuhongdoan@gmail.com
thu-hong.doan@unamur.be
guillaume.berionni@unamur.be

Dr. N. Vanthuyne, Dr. M. Albalat
Aix Marseille Univ, CNRS, Centrale Med, FSCM, Chiropole, Marseille, France

L. Collard
Institute of Condensed Matter and Nanosciences–Molecules
UCLouvain - Place Louis Pasteur 1, Louvain la Neuve, bte L4.01.03

Introduction

Atropisomerism is a type of axial chirality arising from restricted rotation around a single bond connecting two different moieties, typically two aryl rings,[1] such as in the prototypical biaryl and binaphthyl derivatives.[2] Since the seminal Noyori's discovery of asymmetric hydrogenation reactions,[3] biaryl and binaphthyl derivatives found numerous stereoselective synthetic approaches,[4] and applications ranging from catalysis,[5] to materials science,[6] polymers[7] and supramolecular chemistry.[8] Beyond those archetypical atropisomers in which chirality arises from restricted rotation at a C–C bond, axially chiral frameworks based on C–O, C–S and C–N bonds (hetero-atropisomers) are increasingly investigated.[9]

Organoboron compounds such as triarylboranes,[10] are of interest due to their applications in various fields such as in catalysis,[11] anions sensors[12] and material sciences.[13] Due to the vacant p_z orbital at the sp^2 hybridized boron atom, triarylboranes have a trigonal planar geometry around boron with a propeller type arrangement of their aryl rings. Such conformation, paired with the free rotation around C–B bond makes chirality and especially atropisomerism and restricted rotation at their C–B bonds highly challenging.

Following the pioneering work of Mislow on conformational analysis of rotation at C–B bond in triarylboranes,[14] various structural modifications have been performed to slowdown the propeller conformational interconversion, including the introduction of bulky substituents around the boron center, the addition of covalent linkers, or stabilizing π-π interactions, as in the bis-ethyl-bridged borane **A**,[15] the 1,3-diphenylethynyl substituted "blade"-triarylborane **B**,[16] or the 1,1-binathyl-triarylborane **C**, respectively (Figure 1a).[17] Helical chirality in boron-containing helicenes is gaining increasing interest in recent years and the configurationally stable enantiopure compounds **D**-**F** were very recently reported (Figure 1b).[18]

Although atropisomerism at C–B bond was observed in azaborine and azaborinine heterocycles **G**-**H**[19] and in hindered non-biaryl alkyl-amino-boranes **I**,[20] due to slow rotation about a Csp^2–B bond (Figure 1c), and more recently in atropisomeric dative Lewis adducts of triarylboranes with amines,[21] a boron Lewis acid in which chirality solely derived from atropisomerism phenomena at a C–B bond is remaining unknown so far.[22]

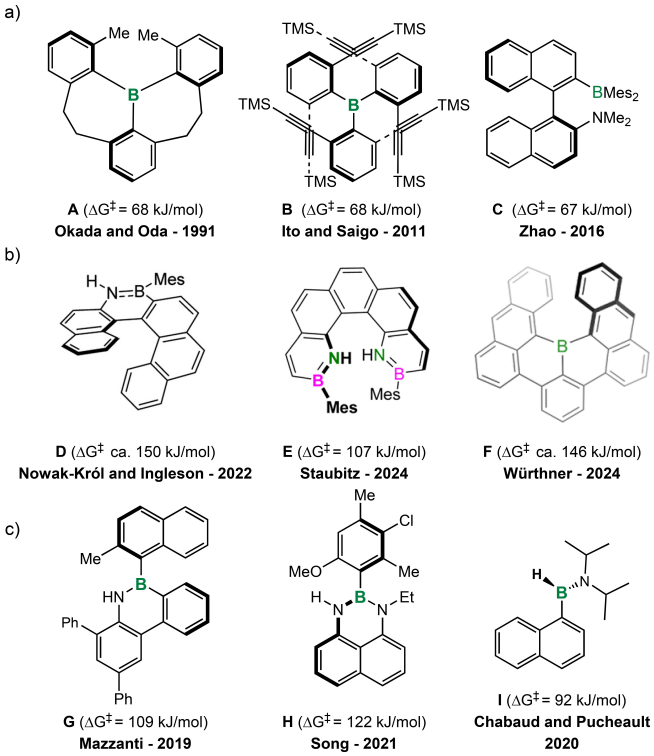

Figure 1. a) Propeller and binaphthyl shaped chiral triarylboranes; b) Helical chiral boron compounds; c) Non-biarylic aminoboronate atropisomers based on restricted rotation around C–B bound in B–N bora-aza heterocycles and amine-boranes. Barriers of interconversion for rotation at the chiral axis are displayed.

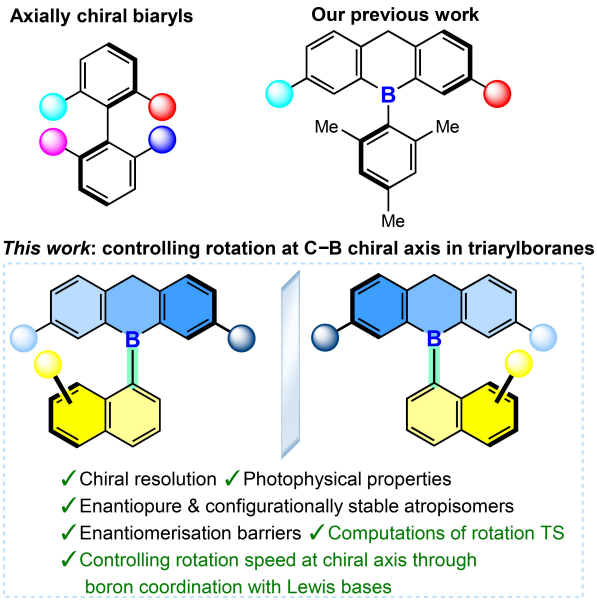

Figure 2. Design of atropisomeric triarylboranes with controlled rotation speed at the C–B axis.

As part of our continuing interest in the synthesis and properties of semi planar and bridged triarylboranes,[23] we now describe the rational development of a new class of asymmetrical triarylboranes according to the following principles (Figure 2):

i) the semi-rigid dihydro-9-bora-anthracenyl unit will annihilate the propeller type interconversion known in classical triarylboranes;

ii) the orthogonal arrangement between the naphthyl and the bora-anthryl moiety should strongly hamper the rotation of these two moieties around the Csp^2–B bond enabling chiral resolution;

iii) proper substitution pattern will enable rotation control around the C–B chirality axis and ensure high enantiomerization barrier;

iv) Unlike in amino-boranes and aza-boronates (Figure 1c), the trivalent boron atom of the triarylborane is a Lewis acid, and interact with Lewis bases, leading to a molecular rotation speed triggered and controlled by the addition of a Lewis base.

These new types of naphthyl-dihydroanthracenyl boranes are to the best of our knowledge, the first triarylboranes displaying atropisomerism. The resolution of enantiomers was achieved through chiral HPLC and their absolute configuration was assigned through X-ray diffraction analysis. Their electronic circular dichroism (ECD), photophysical properties and mechanism of enantiomerization were fully elucidated through advanced NOESY, 1H-TOCSY and variable temperature (VT) - NMR studies, kinetics of isomerization in different solvents, and quantum chemical calculations.

We demonstrated that the steric environment of the boron atom can be controlled through a reversible Lewis base binding, via a mechanism that is reminiscent to allosteric regulation of the rotational speed of molecular motors.[24] This gives access to a controlled rotation speed around the C–B chiral axis through Lewis bases binding at the boron atom, illustrating a new feature of Lewis acid-base chemistry.

Results and Discussion

Synthesis of Non-Symmetrical Triarylboranes

The target asymmetrical boranes **4a**–**m** were synthesized based on our recently reported one-pot synthetic method.[23a] The bis(2-bromophenyl)-methane derivatives **1** were prepared in our group and used as the starting materials for this synthesis (see Supporting Information for details). The Grignard reaction of **1** with Mg^0 powder produced the bis(2-bromomagnesium aryl)-methane intermediates, which then reacted with trimethylborate to give the intermediate boronates **2**. These intermediates were then combined directly with the Grignard reagents **3** to afford the desired triarylboranes **4a**–**m** (Scheme 1). In Scheme 1, naphthyl magnesiumbromide derivatives are shown as examples of the Grignard reagents **3**, which were prepared from the corresponding bromonaphthalenes (see Supporting Information for the other bromoarenes and their preparation). Substitution at position 2' and 8' of the naphthalene scaffold is crucial to enhance the stability of the triarylboranes **4** by

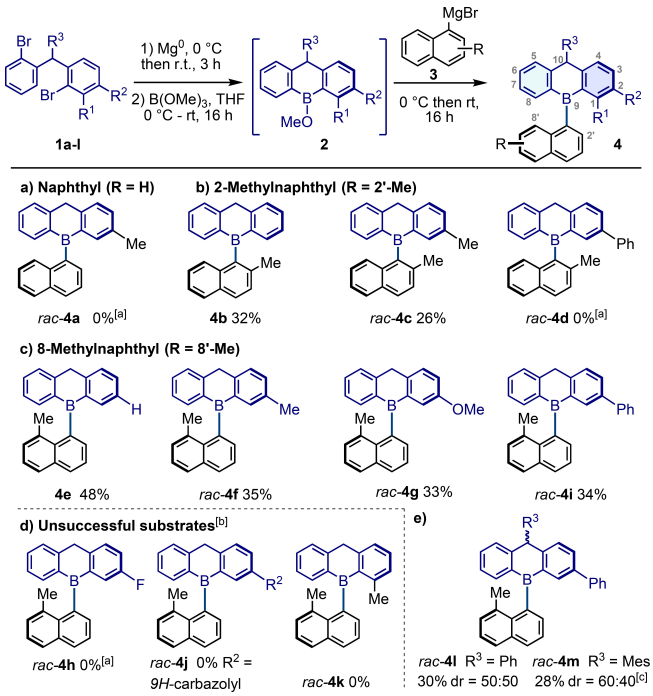

Scheme 1. Synthesis of unsymmetrical sterically hindered triarylboranes **4** via three C–Mg and three C–B bonds formation, and isolated yields after purification by flash-chromatography. [a] These compounds readily decomposed during the purification step into boronic and borinic acids, see the SI, section 7. [b] For other unsuccessful substrates, see the SI. [c] See the NMR-spectroscopic investigations below for the diastereomer structure assignment.

sterically shielding the boron atom, as exemplified by the rapid decomposition of **4a** (confirmed by ^{11}B NMR with the signal at 47.8 ppm, see the SI) into its borinic acid analogue in solution.

With the 2'-methylnaphthyl moiety, compounds **4b** without substituent and **4c** with the methyl group at the C2 position of the dihydro-9-bora-anthracene have been successfully synthesized with overall yields of 32 % and 26 %, respectively (Scheme 1b). Surprisingly, the replacement of the methyl group by the phenyl group on dihydro-9-bora-anthracene scaffold decreased the triarylborane stability and **4d** readily decomposed in boronic and borinic acids by-products (see the SI, section 7).

With the 8'-methylnaphthyl moiety, boranes **4e**–**g** bearing H, Me and OMe group, respectively, were obtained in good yields (Scheme 1c). While a fluorine atom resulted in an unstable borane **4h** which decomposed quickly (as detected by ^{11}B NMR spectroscopy, see SI), the borane **4i** with a phenyl group was isolated in 34 % yield. Replacing the phenyl group by the bulkier moiety as carbazole (**4j**) did not give the desired compound.

When changing the position of the methyl group in the dihydro-9-bora-anthracene scaffold from the C2 (as in **4f**) to the C1, no desired product **4k** was obtained (Scheme 1d). This proved that dihydro-9-bora-anthracene scaffold substituted at C2 are more suitable for the design of the chiral boranes.

Functionalization of the position 10 of the dihydro-9-bora-anthracene scaffold was finally investigated (Scheme 1e) and two boranes **4l** and **4m** with a phenyl and mesityl substituent at the C10 position were obtained in 30 % and 28 % yields, respectively. Further scopes and limitations of this method are detailed in the SI, illustrating that in general bulkier aromatics (carbo[5]helicene, triptycene, anthracene and dinaphtho[2,1-b:1′,2′-d]furan) or conjugated moeties (phenylacetylene, carbazole) are not leading to the triarylboranes formation.

X-Ray Crystallography Investigation

Single-crystals X-ray diffraction crystallographic studies on **4b**, **4e**, **4f**, **4g** and **4i**[25] revealed that the naphthalene unit is nearly perpendicular to the almost flattened dihydro-9-bora-anthracene unit, with the interplanar angles between these two subunits ranging from 77° to 90° (Figure 3).

While the B–C1' bonds are nearly of identical length (~1.58 Å), the angles between B–C1'-C9' (ranging from 127.6° to 128.1°) and R'$_{8'}$-C8'-C9' (ranging from 121.3° to 122.4°) of **4e**–**g** are wider than in **4b** (~120°, Table 1). Likewise, the distance between the B atom and C8' atom of the naphthalene skeleton in the cases of **4e**–**g** and **4i** (average value of 3.2 Å) is longer than in **4b** (2.97 Å) illustrating the steric hindrance of the CH_3 substituent at the C8' peri-position that pushes away the dihydro-9-bora-anthracene scaffold at the other naphthalene *peri*-position in **4e**–**g** and **4i**.

Photophysical Properties in Solution

We then assessed the optical properties of a series of triarylboranes in solution and observed maximum absorptions at ~280 nm with molar extinction coefficient around 35000 $cm^{-1}M^{-1}$ with a small absorption band (ε = 5000 $cm^{-1}M^{-1}$) approaching nearly 350 nm. They exhibited

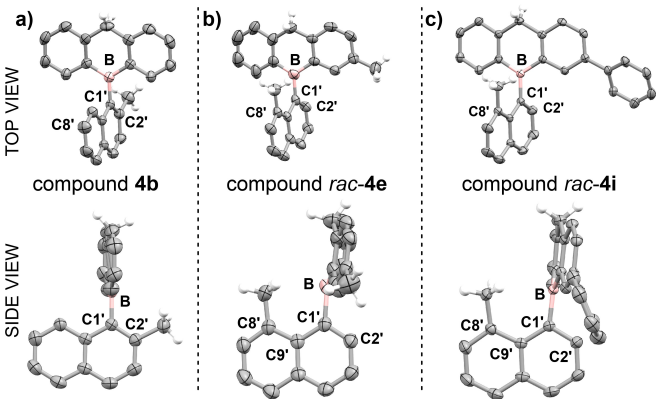

Figure 3. Molecular structures of a) compound **4b**; b) *rac*-**4e** and c) *rac*-**4i**. One of the two enantiomers is shown for *rac*-**4e** and *rac*-**4i**. Non-essential H-atoms have been omitted for clarity. Thermal ellipsoids are set at 30% probability level. For the X-ray structure of **4g**, see Figure 8.

Table 1: Selected crystallographic parameters of **4b, 4e–g** and **4i**.[a]

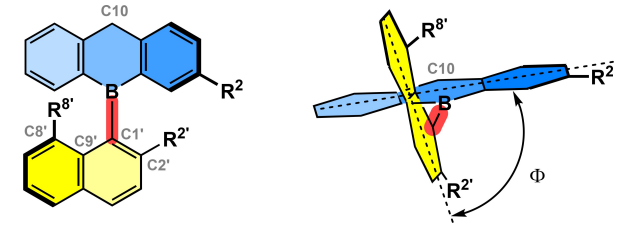

Comp.	R^2	$R^{2'}$	$R^{8'}$	Φ (°)	B–C1' (Å)	B–C1'–C9' (°)	$R^{8'}$–C8'–C9' (°)
4b	H	CH_3	H	84.0	1.574 [b]	119.7 [b]	119.1 [b]
4e	H	H	CH_3	78.0	1.571(2)	127.7	122.2
4f	CH_3	H	CH_3	81.7	1.584 [b]	128.1	121.3
4g	OCH_3	H	CH_3	89.7	1.577(2)	127.5	122.0
4i	Ph	H	CH_3	77.3	1.576(2)	127.6	122.4

[a] All data collected at 100 K unless otherwise stated. Φ defined the interplanar angle between the 9-boraanthryl and naphthyl scaffolds. [b] Average on several crystallographically independent structures with very similar bond lengths and angles values.

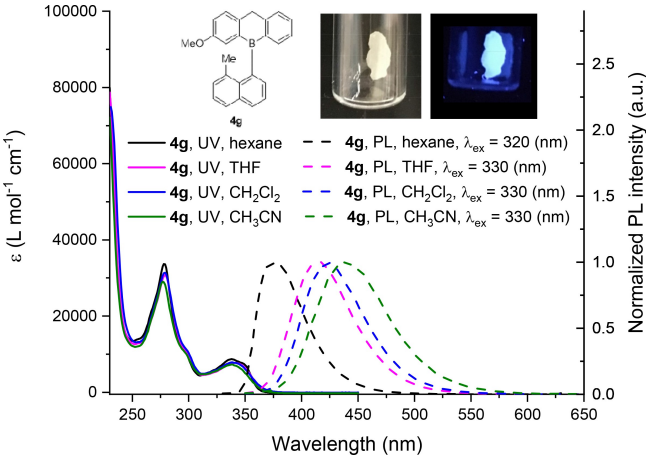

Figure 5. UV/Vis absorption spectra (straight lines) and photoluminescence spectra (dashed lines) of rac-**4g** in hexane, THF, CH_2Cl_2 and CH_3CN with the inserted photos of rac-**4g** in the solid state under white light (left) and UV light (right).

blue-violet emission band with fluorescence at *ca.* 450 nm in CH_2Cl_2 (Figure 4).

More interestingly, the fluorescence spectra of these triarylboranes were strongly influenced by the solvent polarity, as illustrated by the emission wavelength of **4g** shifting of nearly 100 nm when going from *n*-hexane to acetonitrile (Figure 5). Very large Stokes shifts in the range of 3×10^3 to 7×10^3 cm^{-1} were observed (See the SI, section 14).

NMR-Spectroscopic Investigation

Two diagnostic signals on the ^1H NMR spectra were those of the two hydrogen atoms at the methylene position C10 of the dihydro-9-bora-anthracene scaffold in the compounds **4** (see the Supporting Information for their NMR spectra). At 25 °C in $CDCl_3$ a singlet integrating for two protons is observed at ~4.65 ppm for **4b** and **4c** illustrating that the dihydro-9-bora-anthracene and the naphthyl subunits were insufficiently substituted and steric repulsions were not sufficient to slow-down the rotation the B–C1' bond below the NMR timescale. On the other hand, they split into indicative diastereotopic AB-system doublets at 4.60 (J_{AB} = 25 Hz, δ_A = 4.61 ppm, δ_B = 4.58 ppm), 4.55 (J_{AB} = 20 Hz, δ_A = 4.56 ppm, δ_B = 4.53 ppm), 4.54 (J_{AB} = 25 Hz, δ_A = 4.55 ppm, δ_B = 4.52 ppm) and 4.64 (J_{AB} = 24 Hz, δ_A = 4.64 ppm, δ_B = 4.61 ppm) in the cases of **4e**, **4f**, **4g** and **4i**, respectively (see Figure 6). Thus, switching the position of methyl group in the naphthalene moiety from the C2' to C8' position considerably slows down the rotation speed around the C–B bond. Interestingly, in the case of **4i**, the more split AB-system signals in toluene-d_8 than in $CDCl_3$ are the first evidence of the influence of the solvent on the rotation (Figure 6).

Surprisingly, compound **4m** was obtained as a diastereoisomeric mixture of 60:40 after synthesis according to ^1H NMR integrals and then confirmed by HPLC (see the Supporting Information for details, section 6). This suggested that the borylation might be diastereoselective. The major isomer has been attributed a *cis*-configuration (where both mesityl and the naphthyl units are located on the same side with respect to the anthryl scaffold), as proven by 1D-gemstone, ^1H-^1H NOESY and 1H-TOCSY NMR studies (see the SI, page 85). An attempt to study the stereodynamic behaviors of the selected compounds **4b**, **4c** and **4i** by the variable temperature NMR analysis has been carried out (see SI, section 6). No coalescence or peak broadening was detected even at 100 °C in toluene-d_8 in the case of **4i**, suggesting that the sterically hindered environment around the C–B axis is preventing the rotation of the naphthyl and dihydro-9-bora-anthracenyl units, and thus that chiral resolution is possible.

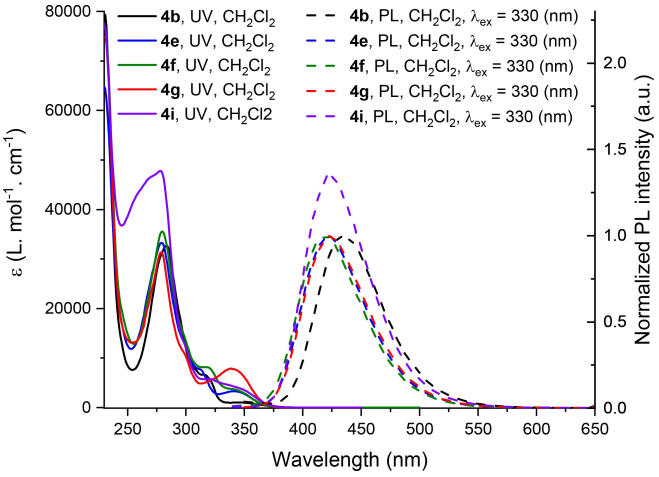

Figure 4. Absorption and emission spectra of **4b**, **4e**, **4f**, **4g** and **4i** in solution in CH_2Cl_2.

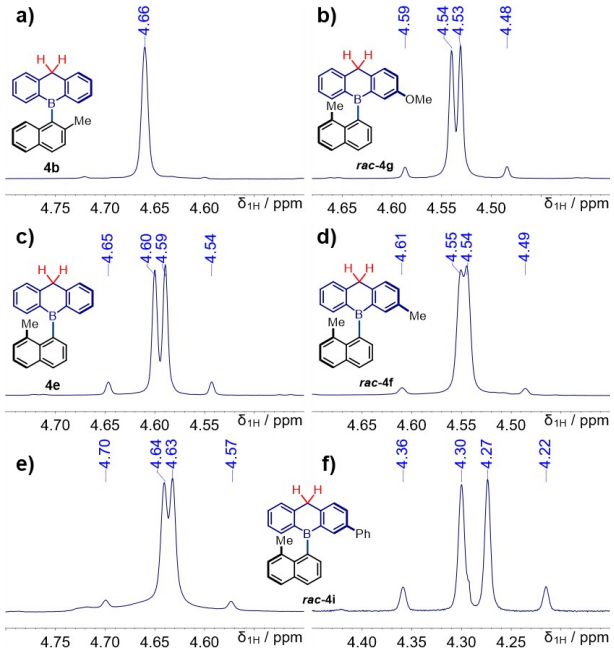

Figure 6. Zoom of the ^{1}H NMR spectra of: a) **4b** in $CDCl_3$; b) ***rac*-4g** in $CDCl_3$; c) **4e** in $CDCl_3$; d) **rac-4f** in $CDCl_3$; e) **rac-4i** in $CDCl_3$; f) **rac-4i** in toluene-d_8 showcasing the signals of the two diastereotopic hydrogens at position C10.

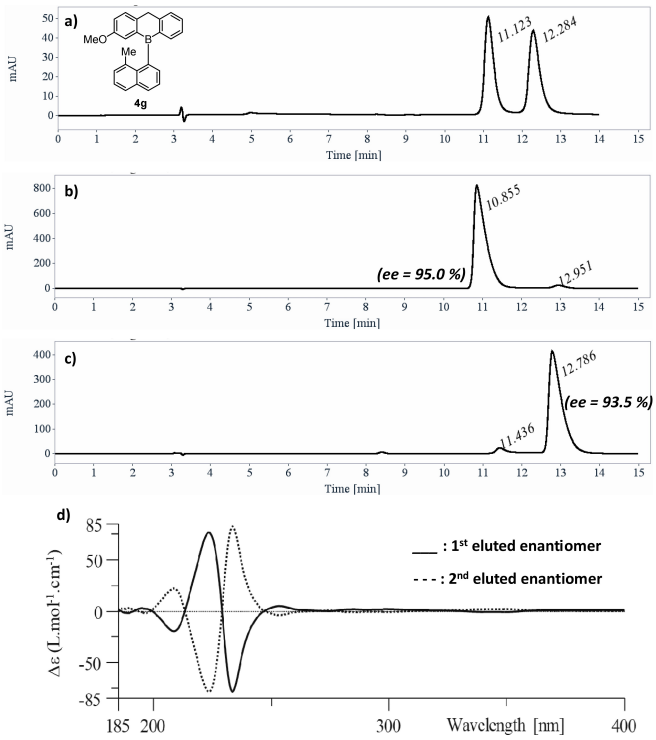

Figure 7. CSP-HPLC chromatogram on Chiralpak IB N-5 (*n*-heptane/dichloromethane 95 : 5) of the atropisomeric triarylborane **rac-4g** with retention times (in minutes) and their absorbance at 254 nm. The difficult stabilization of the column with ethanol free eluent mixtures explains the slight variation in retention times, see the SI. b) and c) CSP-HPLC chromatogram of the isolated enantiomers with the corresponding ee; d) ECD spectra of the first eluted (R_a-**4g**, bold line) and the second eluted (S_a-**4g**, dashed line) enantiomers of **4g** recorded in solution in *n*-hexane.

Chiral Resolution by Preparative Chiral HPLC Separation and Absolute Configuration Determination

The separation of enantiomers in the racemic mixture of **4f**, **4g**, **4i**, **4l** and **4m** were done by preparative HPLC on chiral stationary phase CSP-HPLC (see detailed conditions in SI).

Each enantiomer of **4f**, **4g**, **4i**, **4l** and **4m** were obtained with high enantiopurity (enantiomeric excess (*ee*) from 93.5 % to 99.5 %), as illustrated in the CSP-HPLC chromatogram for the separation of both enantiomers of **4g** and their corresponding ECD spectra exhibiting mirror signals (Figure 7). The full resolution data of the other compounds **4f**, **4i**, **4l** and **4m** are shown in Supporting Information (Section 9). The chiral resolution was not possible in the case of **4c**, indicating that the resulting enantiomers interconvert rapidly, as confirmed by the quantum-chemical calculations (see infra).

We then determined the absolute configuration of each resolved enantiopure samples by X-ray diffraction. In the case of **4f** the crystallization of either enantiomer was found to be slower than the interconversion process and despite multiple attempts, the single crystals have been obtained with a maximum of 80 % ee (see the SI). In contrast, both enantiomers of **4g** crystallized rapidly in *n*-hexane at −10 °C, preventing racemization and affording single-crystals suitable for X-ray diffraction analysis. This allowed us to attribute the absolute configuration (R_a) to the first and (S_a) to the second eluted enantiomer of **4g** and we attributed their optical rotations $[\alpha]_D$ (Figure 8).

Compound **4l** with one stereogenic carbon atom at C10 and the C–B axis of chirality displayed two pairs of

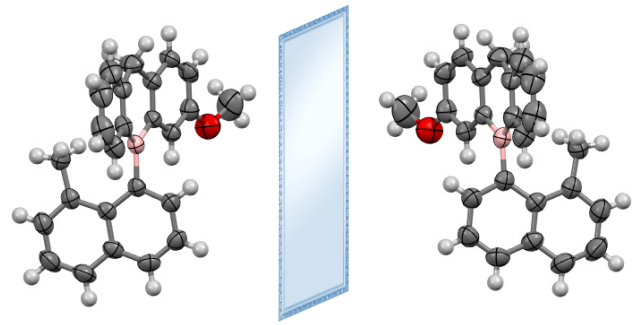

Figure 8. Molecular structures of both enantiomers of **4g**, optical rotations are displayed at 589 nm at 25 °C. Thermal ellipsoids are set at 50 % probability level, crystal structure determination at 100 K, see details in the SI.

enantiomers, **4l A+/A−** and **4l B+/B−**, which can be highlighted by CSP-HPLC with UV and circular dichroism detection at 254 nm (Figure 9a). According to this chiroptical detection, the first eluted peak, named **4l A−**, is the enantiomer of the second eluted peak **4l A+**, and the third eluted peak **4l B+** is the enantiomer of the last peak **4l B−**.

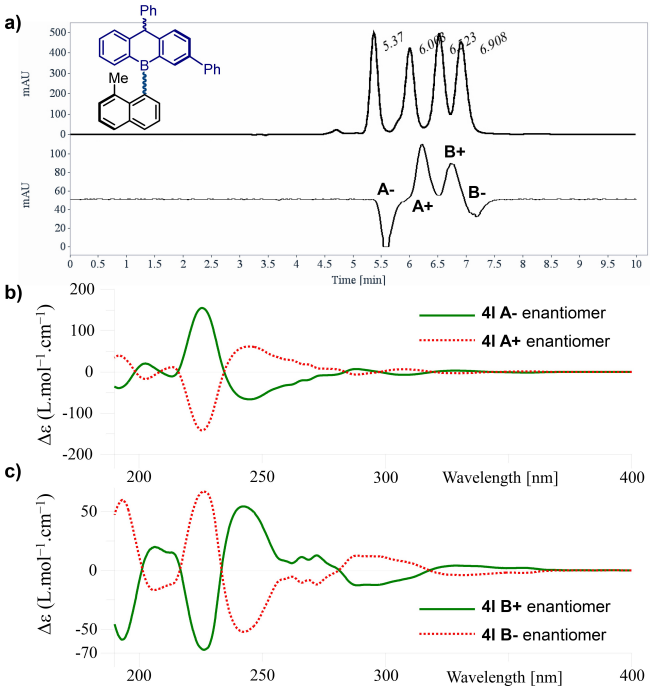

Figure 9. a) CSP-HPLC chromatogram on a Chiral Art Cellulose SZ (heptane/dichloromethane 90:10) of racemic atropisomeric triarylborane pairs **4l**, UV detection and circular dichroism detection at 254 nm.; b) and c): ECD spectra of the two pairs of enantiomers (see Supporting Information section 9 for the separation of the four stereoisomers of **4m**, page S113).

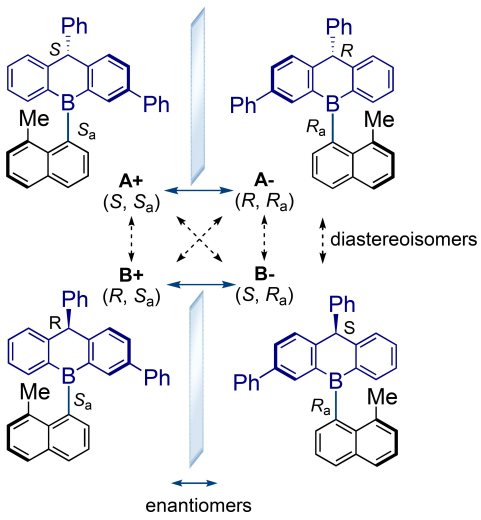

Figure 10. Absolute configuration of the four stereoisomers of **4l** as determined by comparisons of the experimental and ECD spectra simulated by quantum-chemical calculations. See structural assignment in the SI.

The reported signs correspond to the signs given by the circular dichroism detector at 254 nm and also in this case to the sign of the $[\alpha]_D$ (see the SI, section 10). The four isomers are obtained by preparative CSP-HPLC with *de* higher than 97 % and ee > 99.5 % (see the SI, section 9, p S99).

The electronic circular dichroism (ECD) spectra of the first resolved enantiomer pair A+/A− of **4l** show a typical mirror-image relationship (Figure 9b) with a maximum at $\lambda = 225$ nm, ($\Delta\varepsilon = \pm 150\ M^{-1}cm^{-1}$). The second resolved enantiomer pair B+/B- of 4 l showed to mirrored bands of smaller but similar amplitude ($\Delta\varepsilon = \pm 60\ M^{-1}cm^{-1}$) at $\lambda = 225$ and 245 nm (Figure 9c).

To assign the absolute configuration of all four stereoisomers, we computed their ECD spectra by TD-DFT using *n*-hexane as solvent with the PCM solvation model including the 60 lowest energy transitions. The ECD spectra of **4f**, **4g**, **4i** were also computed and enabled us to assign the absolute configuration of their resolved enantiomers. The calculations reproduced well the general shape of the experimental ECD spectra, except at the lower energy range (< 200 nm, see the experimental and simulated ECD spectra in the SI, part 15).

This allowed us to establish that the absolute configuration of the first eluted enantiomers of **4l**, noted A− is (*R*, R_a), and that of the second eluted enantiomer of **4l**, noted to A+ is (*S*, S_a). The second enantiomer pairs B+/B− eluting at high retention time was attributed to the (*R*, S_a) and (*S*, R_a) absolute configurations, respectively (Figure 10).

Solvent Dependent Rotation Rates at C– Chiral Axis

For enantiomer pairs **4f**, **4g** and **4i**, the rotation around B–C1′ bond results in enantiomerization, while it results in diastereomerization for **4l** and **4m**. Nevertheless, the ratio between the diastereomers **4lA**/**4lB** and **4 mA**/**4mB** is 1/1 at the thermodynamic equilibrium in all tested solvents, so that there is only one diastereomerization rate which corresponds to the rotation rate at the C–B chiral axis. The kinetics of isomerization of the boranes **4f**, **4g**, **4i**, **4l** and **4m** have been studied in several solvents (see Table 2) and first order kinetics were observed and used to determine the rotation rates.

In apolar solvents like hexane and heptane with nearly identical polarities, similar rotation rates k_{rot}, $\triangle G^{\ddagger}$ and half-time $t_{1/2}$ were observed, as expected. In particular, the long half-time of enantiomerization in these two solvents (11.8 and 11.3 days, respectively) confirms that **4f** is a configurationally stable atropisomer with extremely slow racemization in solution. This is in respect to the requirement of $t_{1/2}$ > 1000 seconds to be an atropisomer.[26]

The enantiomerization process is about ~1.7 times faster in CH_2Cl_2, the more polar solvent, resulting a decrease of the half-time of enantiomerization from about 11 to 7 days. Notably, the enantiomerization is about 2 times slower with the decreased temperature of 5 °C in both cases (in hexane and CH_2Cl_2).The isomerization of **4g**, **4i** and **4l** was also observed at 25 °C in hexane, heptane and dichloromethane, with half-life time in a range from 3.3 to 17.0 days, but temperature has to be increased at 98 °C to epimerize **4m** (Table 2). At 25 °C, the half-life time is estimated at several decades for **4m**. Thus, the slow rotation proved that compounds **4g**, **4i**, **4l** and **4m** are highly configurationally stable atropisomers.

The group of three compounds **4f**, **4g** and **4i** bearing different substituents at the position 2 of the 9-boraanthra-

Table 2: Experimental kinetic parameters of isomerization of compounds **4f, 4g, 4i, 4l** and **4m** (see the Supporting Information for the ■■■Missing text? Please check. Thank you.■■■

Comp	Solvent	Temp (°C)	k_{rot} (s^{-1}) [a]	$\triangle G^{\neq}$ [a] (kJ.mol^{-1})	$t_{1/2}$ [b] (days)
4f	Hexane	25	3.38×10^{-7}	108.2	11.8
	Heptane	25	3.55×10^{-7}	108.1	11.3
	CH_2Cl_2	25	5.74×10^{-7}	106.9	7.0
	Hexane	20	1.72×10^{-7}	108.0	23.4
	CH_2Cl_2	20	2.83×10^{-7}	106.8	14.2
4g	Heptane[c]	25	6.62×10^{-7}	106.6	6.1
	CH_2Cl_2 [d]	25	1.23×10^{-6}	105.1	3.3
4i [e]	Hexane	25	1.26×10^{-6}	105.0	3.2
	Heptane	25	1.10×10^{-6}	105.3	3.7
	CH_2Cl_2	25	1.06×10^{-6}	105.4	3.8
	Toluene	25	2.32×10^{-6}	103.4	1.7
	1,2-DCE	25	6.69×10^{-6}	100.8	0.6
	Chloro-benzene	25	1.11×10^{-6}	105.3	3.6
4l(A+)	Heptane	25	2.35×10^{-7}	109.2	17.0
	CH_2Cl_2	25	3.11×10^{-7}	108.5	12.9
4m(A1)	Heptane	98	4.37×10^{-6}	127.6	0.92

[a] Calculated by decay of enantiomeric or diastereomeric excess by HPLC. [b] Half time for isomerization, determined using the following equation: $t_{1/2}=\ln(2)/k_{rot}$. [c] k_{rot} in hexane are similar within 10% than those in heptane, see the SI. [d] Same results obtained in CH_2Cl_2 stabilized with EtOH or amylene. [e] The enantiomerization was instantaneous in Et_2O, THF, acetone, CH_3CN and EtOH.

cene scaffold was considered. The similar significant effect of solvents with different polarities on the rotation of **4f** can be clearly seen in the case of **4g** containing the methoxy group. Nevertheless, minor influence of solvents was found in the case of **4i** with the phenyl substituent due to comparable rate constants k_{rot} values.

The aim of inserting a phenyl substituent at the C7 position of dihydro-9-bora-anthracene scaffold was to prevent the rotation at the C–B axis by steric repulsions and thus to increase the enantiomerization energy barriers. Surprisingly rotation is about 3.7, 3.1 and 1.8 times faster for the enantiopure **4i** (bearing a Ph group), than for **4f** (bearing a Me group) in heptane, hexane and CH_2Cl_2, respectively. In addition, among the three derivatives **4f**, **4g** and **4i**, the **4i** has the lowest rotation barrier of 105 (kJ.mol^{-1}) in hexane. Faster enantiomerizations (about 1.8 times) and lower rotation barriers of the **4g** enantiomer with methoxy group were determined in comparison to the one of **4f** bearing a methyl group.

In contrast, a phenyl group at the C10 position of the 9-boraanthracene scaffold as the enantiopure **4l(A$^+$)** was shown to enhance the stabilization of the enantiomer by about 5.6, 4.6 and 3.4 times in heptane, hexane and CH_2Cl_2, respectively, compared to **4i** without phenyl group at the C10 position. Thus, enantiopure **4l(A$^+$)** displays higher rotation barrier (109 kJ.mol^{-1}) in comparison to **4i**, **4f** and **4g**.

These results indicate that the modification of the groups at the C10 position is more efficient than the change of the substituents at the position 2 of the dihydro-9-bora-anthracene scaffold in the purpose of preserving the configuration stability. This effect is even more evident in the case of **4m**, where the introduction of a mesityl substituent at the C10 position was found to increase the rotation barrier up to 128 kJ.mol^{-1}.

Quantum Chemical Investigation

Quantum chemical calculations were performed to elucidate the enantiomerization mechanism of representative triarylboranes, which occurs through rotation around the B–C1' stereogenic axis. Density Functional Theory was employed, with the ωB97X-D[27,28] exchange-correlation functional, the 6-311+G(d,p) basis set, and the implicit IEFPCM[29,30] solvent (heptane) model for geometry optimisation, energies calculations. All calculations were performed using Gaussian 16.[31]

The minimum energy geometries of the reactants and products are characterized by the near orthogonality between the naphthyl and dihydro-9-bora-anthryl scaffold connected through a planar trivalent boron atom, as observed in solid-state structures by XRDC. On the other hand, the transition state (TS) geometries are strongly distorted with an out of plane, bent trigonal environment around the B atom (Figure 11).

Conformational analyses of the TSs showed that in **4c** the dihydro-9-bora-anthryl and naphthyl scaffolds are lying nearly coplanar, with a TS energy 104 kJ/mol higher than the equilibrium structure. This large energy barrier is related to the steric H–H repulsion (distances around 2.2 Å) inducing a bent V-shape structure on the boraanthryl scaffold. Still, the steric repulsions are stronger on **4f** and **4i** because the methyl group lies at the $R^{8'}$ naphthyl position. Consequently, their interconversion energy barriers reach 128 and 129 kJ.mol^{-1}, respectively. This energy rise is also associated with the increase of the C1-C1' steric hindrance, which disfavours a coplanar transition state and slightly increases the dihydro-9-bora-anthryl out of plane angle to 72°. The theoretical interconversion barriers are ~20 kJ.mol^{-1} larger than the experimental ones, however, the values are within the accuracy of the method and show the right trend. Thus, interconversions take place through perpendicular TSs, where the boranthracenyl and naphthyl units are perpendicular to each other.

Replacing the methyl (**4f**) with a phenyl (**4i**) at C2-position neither significantly impacts the barrier to isomerization nor the TS structure. This behaviour is ascribed to *i*) the strong steric effects located near the B–C1' stereogenic axis and *ii*) that different R^1 substituents impact a little the bending energy of the dihydro-boranthracenyl moiety. As in Feringa's molecular motors[32] featuring a highly flexible thioanthryl backbones undergoing large twisting/folding to enable rotation of the rotor and the stator around the C–C bond, the near planar boranthracenyl stator in **4** is severely folding with a folding angle going up to 72° (Figure 11F) for minimizing the steric repulsions during the rotation at the C−B bond. This however enables an increased π-conjugation length and extensive electron-delocalization through the trivalent boron atom due to the planarization of both π-systems.

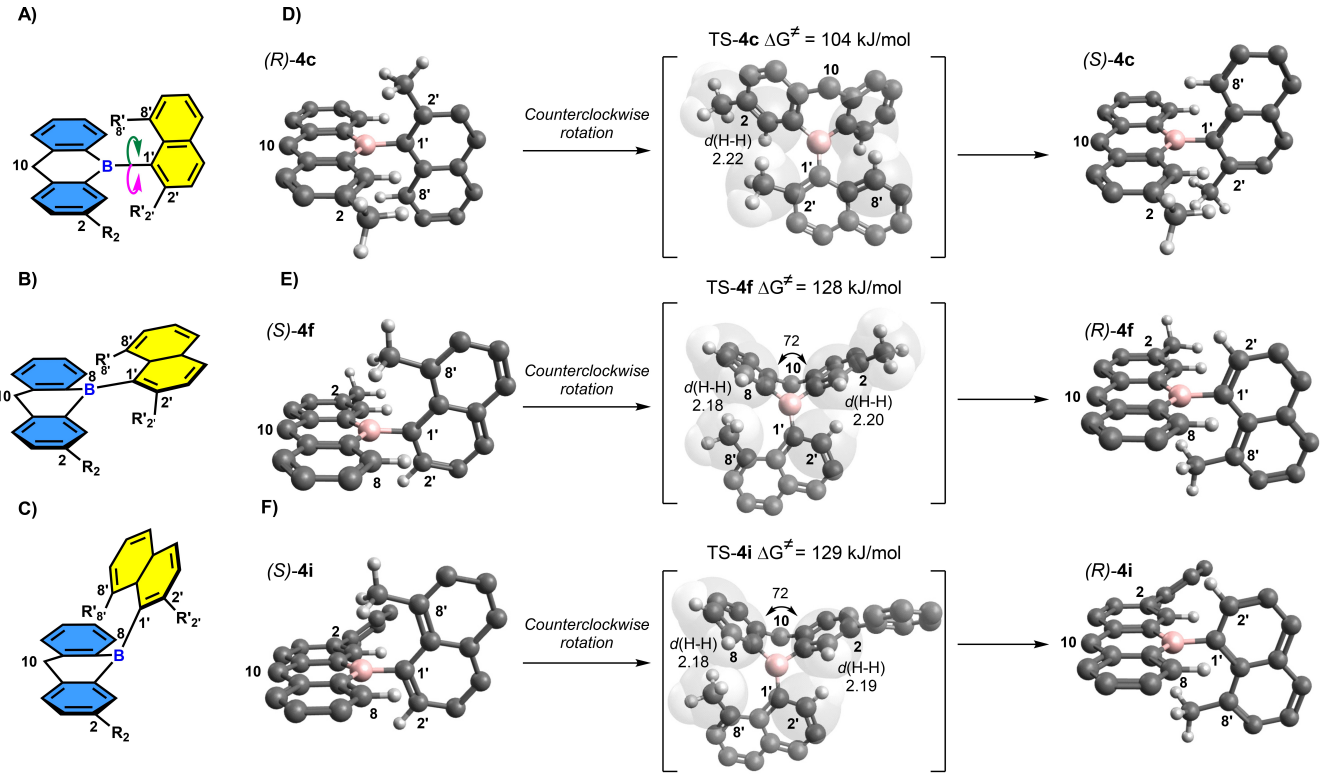

Figure 11. A) Enantiomers interconversion via clockwise (green arrow) or counterclockwise (purple arrow) rotation around C–B bond; B) and C): transition state models depending on the position of the substituent on the naphthyl group (R_2 = Me or Ph, R'$_{2'}$ = H or Me and R'$_{8'}$ = H or Me); D), E) and F): Optimized structures of the reactants, transitions states and products for the interconversion of **4c**, **4f** and **4i**, calculated at ωB97X-D/6–311 + G(d,p) level in implicitly heptane solvent. Activation free energies, selected distances (in Angstrom) and angles (in degree) are displayed.

Lewis Base Assisted C–B Rotation

Whereas the trivalent boron atom must undergo a strong distortion from the trigonal planar geometry to reach the TS of rotation, we envisioned that adding a Lewis base will assist the rotation process, by decreasing the TS energy by forming reversibly, not in the ground state, but exclusively in the TS, a boron Lewis acid-base adduct with a tetracoordinated boron atom.

Thus, addition of ethanol (0.05 %, v/v) to the solution of one enantiomer **4f** in hexane increased rotation speed of a factor 23, representing a decrease of configurational stability of $t_{1/2}$ from 23.4 to 1.0 day (see Table 3), and a 7.6 kJ.mol^{-1} decrease of $\triangle G^{\neq}$. When the amount of ethanol was increased to 0.5 %, a dramatic enantiomerization acceleration of about 3000 times was observed, corresponding to a $t_{1/2}$ of only 12 minutes. The experimental enantiomerization barrier decreased from 108.0 to 88.6 kJ.mol^{-1}.

Similar investigations were done by addition of CH_3CN and EtOH (polarity of 0.460 and 0.654) to the solution of one enantiopure **4f** in CH_2Cl_2. The enantiomerization was significantly faster (about 98 and 229 times) with the presence of 0.5 % and 1 % of CH_3CN in the CH_2Cl_2 solution. A similar trend can be seen when replacing CH_3CN by EtOH. Interestingly, although the racemization of one enantiomer **4f** is faster in CH_2Cl_2 than in hexane, it is 20 times slower in the presence of 0.5 % EtOH.

Table 3: Solvent dependent kinetic parameters of enantiomerization for **4f**.

Solvent	T (°C)	k_{enant} [a] (s^{-1})	$\triangle G^{\neq}$ [a] (kJ.mol^{-1})	$t_{1/2}$ [b]
Hexane	20	1.72×10^{-7}	108.0	23.4 d
Hexane + 0.05 % EtOH	20	4.01×10^{-6}	100.4	1.0 d
Hexane + 0.50 % EtOH	20	5.05×10^{-4}	88.6	12 min
CH_2Cl_2	20	2.83×10^{-7}	106.8	14.2 d
CH_2Cl_2 + 0.50 % CH_3CN	20	2.78×10^{-5}	95.6	3.5 h
CH_2Cl_2 + 1.00 % CH_3CN	20	6.48×10^{-5}	93.6	1.5 h
CH_2Cl_2 + 0.50 % EtOH	20	2.48×10^{-5}	95.9	3.9 h
CH_2Cl_2 + 1.00 % EtOH	20	9.70×10^{-5}	92.6	1.0 h

[a] Calculated by decay of enantiomeric excess by HPLC. [b] Half time for enantiomerization, determined using the following equation: $t_{1/2} = \ln(2)/k_{enant}$.

Quantum chemistry calculations of the Gibbs free energies of **4f** in ethanol show a high molecular distortion around the B–C bond in TS to achieve the rotation with a barrier of 125 kJ.mol^{-1} (Figure 12, from (b) to (a)). When coordinated with an explicit EtOH molecule, Lewis acid-base interaction between the boron atom and oxygen atom of the EtOH molecule are facilitated (shorter B···O bond, Figure 12c-d), allowing solvent-assisted rotation paths, resulting in a greatly reduced $\triangle G^{\neq}$ = 32 kJ.mol^{-1} barrier. Therefore, a 10 kJ.mol^{-1} decrease in the TS Gibbs free energy is observed from the non-assisted rotation process to

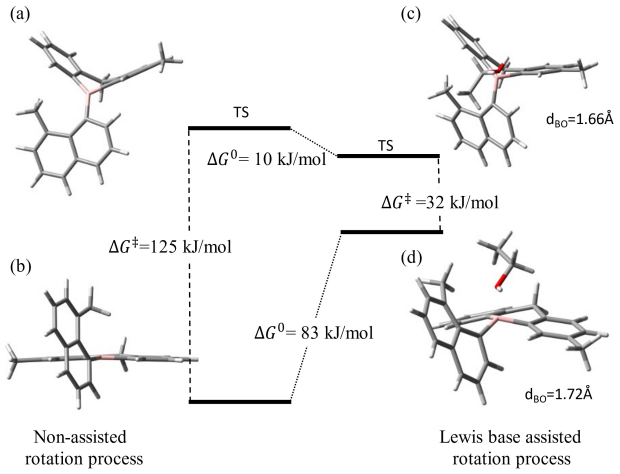

Figure 12. Relative Gibbs free energy diagram illustrating the enantiomerization process for **4f** in ethanol. (a) and (b) represent the transition and ground state structures, respectively, for non-assisted process, while (c) and (d) represent the transition and ground state structures, respectively, for ethanol (EtOH) assisted process. All calculations (energy minima and saddle point structures and free energies) were computed at the ωb97X-D/6–311 + G(d,p) level of theory at 25 °C. The solvent (ethanol) effects were accounted for using IEFPCM.

the Lewis-base assisted one (Figure 12 (a) and (c)). A similar effect is observed for **4i**, in which the assisted process leads to $\triangle G^{\neq} = 31$ kJ.mol^{-1} (See the Supporting Information section 15). Alternatively, the solvent effects were analysed in two other manners. First, in heptane approximated by the IEFPCM model plus one explicit EtOH molecule, it shows a $\triangle G^{\neq}$ increase to 41 kJ.mol^{-1} and 38 kJ.mol^{-1} for **4i** and **4f**, respectively, indicating that the electrostatic environment slightly affects the enantiomerization process.

Secondly we computed the profile for **4f** in acetonitrile (at the IEFPCM level), including or not one explicit CH_3CN molecule. The non-assisted process has again a $\triangle G^{\neq} =$ 125 kJ.mol^{-1}. The CH_3CN assisted process is more favorable and shows a $\triangle G^{\neq} = 8$ kJ.mol^{-1} barrier, indicating that explicit interaction of solvent molecules with the boron atom plays a crucial role in the rotation dynamics. This lower barrier is attributed to the linear shape of CH_3CN, which reduces steric interactions compared to EtOH (See energies in the SI, section 15). This is consistent with our experimental observations that the enantiomerization is nearly instantaneous in CH_3CN and EtOH and other Lewis basic solvents (Table 2).

Conclusion

Unprecedented atropisomers in the triarylboranes family with a controllable rotation at C–B chiral axis were designed and resolved. Quantum chemical calculations revealed that the formation of a Lewis acid/base adduct is stabilizing the TS by avoiding transiting through a highly distorted trigonal boron atom environment strongly pyramidalized to avoid steric interactions between the rotor (naphthyl) and stator (dihydroboraanthracenyl) subunits. The rationalization of this observation can explain the propeller interconversion strongly dependent to the solvent basicity observed by Saigo and co-workers on the configurationally stable propeller triarylboranes.[16] We are currently exploring the chiro-optical properties and investigating structure-properties relationships between the Lewis base nature and chirality on the control of the rotation at the C–B chiral axis in triarylboranes.

Acknowledgements

We acknowledge the Namur Institute of Structured Matter (NISM) and the Fond National de la Recherche Scientifique (FRS-FNRS) for financial support (grant Numbers: F.4513.18 and T.0012.21 (G.B), U.G006.15 (B.C.), U.G018.19 (B.C.), RW/GEQ2016 (B.C., WR and FNRS) and 1610468 (B.C., WR), and Chargé de recherche research grant for A.C (1.B.087.21F)). Prof Raphaël Robiette (UCLouvain) is gratefully acknowledged for his expertise in quantum chemical calculation and Maxence Bonnevial for the critical reading of the manuscript. The calculations were performed on the computers of the Consortium des Équipements de Calcul Intensif and particularly those of the Technological Platform of High-Performance Computing, which are supported by the FNRS-FRFC, the Walloon Region, and the University of Namur. TNR is a postdoctoral researcher of the Fonds de la Recherche Scientifique – FNRS. We thank the PC2 (UNamur) and UCLouvain platforms for access to all characterization instruments and the European Research Council (ERC, B-yond, grant agreement no. 101044649) for financial support.

Conflict of Interest

The authors declare no conflict of interest.

Data Availability Statement

The data that support the findings of this study are available in the supplementary material of this article.

Keywords: Atropisomerism · Boranes · Chirality · Dynamic stereochemistry · C–B stereogenic axis

[1] a) *Atropisomerism in Asymmetric Organic Synthesis: Challenges and Applications* (Eds.: S. Takizawa, M. Salem), **2025**, Wiley-VCH; b) M. Mancinelli, G. Bencivenni, D. Pecorari, A. Mazzanti, *Eur. J. Org. Chem.* **2020**, *27*, 4070; c) E. Kumarasamy, R. Raghunathan, M. P. Sibi, J. Sivaguru, *Chem. Rev.* **2015**, *115*, 11239.

[2] a) J. Kee, Cheng, S.-H. Xiang, S. Li, B. Tan, *Chem. Rev.* **2021**, *121*, 4805; b) J. Wencel-Delord, A. Panossian, F. R. Leroux, F. Colobert, *Chem. Soc. Rev.* **2015**, *44*, 3418; c) B. Zilate, A. Castrogiovanni, C. Sparr, *ACS Catal.* **2018**, *8*, 2981; d) I.

Alkorta, J. Elguero, C. Roussel, N. Vanthuyne, P. Piras, *Adv. Heterocycl. Chem.* **2012**, *105*, 1.
[3] a) A. Miyashita, A. Yasuda, H. Takaya, K. Toriumi, T. Ito, T. Souchi, R. Noyori, *J. Am. Chem. Soc.* **1980**, *102*, 7932; b) R. Noyori, T. Ohkuma, *Angew. Chem. Int. Ed.* **2001**, *40*, 40; *Angew. Chem.* **2001**, *113*, 40.
[4] a) S. Choppin, J. Wencel-Delord, *Acc. Chem. Res.* **2023**, *56*, 189; b) G. Bringmann, A. J. Price Mortimer, P. A. Keller, M. J. Gresser, J. Garner, M. Breuning, *Angew. Chem. Int. Ed.* **2005**, *44*, 5384.
[5] a) D. Parmar, E. Sugiono, S, S. Raja, M. Rueping, *Chem. Rev.* **2014**, *114*, 9047; b) S. Brandes, B. Niess, M. Bella, A. Prieto, J. Overgaard, K. A. Jørgensen, *Chem. Eur. J.* **2006**, *12*, 6039.
[6] a) L. Pu, *Chem. Rev.* **2004**, *104*, 1687; b) J. M. Cox, I. M. Walton, J. B. Benedict, *J. Mater. Chem. A.* **2016**, *4*, 4028.
[7] a) K. Zhang, Z. Shang, C. J. Evans, L. Han, H. Ishida, S. Yang, *Macromolecules* **2018**, *51*, 7574; b) B. Paul, G. L. Butterfoss, M. G. Boswell, M. L. Huang, R. Bonneau, C. Wolf, K. Kirshenbaum, *Org. Lett.* **2012**, *14*, 926.
[8] S. Maguire, G. Strachan, K. Norvaiša, C. Donohoe, L. C. Gomes-da-Silva, M. O. Senge, *Chem. Eur. J.* **2024**, *30*, e202401559.
[9] a) G.-J. Mei, W. L. Koay, C.-Y. Guan, Y. Lu, *Chem* **2022**, *8*, 1855; b) R. Costil, A. J. Sterling, F. Duarte, J. Clayden, *Angew. Chem. Int. Ed.* **2020**, *59*, 18670; *Angew. Chem.* **2020**, *132*, 18829; c) L. Jin, Q.-J. Yao, P. P. Xie, Y. Li, B.-B. Zhan, Y.-Q. Han, X. Hong, B.-F. Shi, *Chem* **2020**, *6*, 497; d) C. Defieber, H. Grützmacher, E. M. Carreira, *Angew. Chem. Int. Ed.* **2008**, *47*, 4482; *Angew. Chem.* **2008**, *120*, 4558.
[10] a) S. M. Berger, M. Ferger, T. B. Marder, *Chem. Eur. J.* **2021**, *27*, 7043.
[11] a) J. L. Carden, A. Dasgupta, R. L. Melen, *Chem. Soc. Rev.* **2020**, *49*, 1706; b) I. Saridakis, I. Klose, B. T. Jones, N. Maulide, *JACS Au* **2024**, *4*, 3358; c) Y. Hisata, T. Washio, S. Takizawa, S. Ogoshi, Y. Hoshimoto, *Nat. Commun.* **2024**, *15*, 3708; d) D. W. Stephan, G. Erker, *Angew. Chem. Int. Ed.* **2015**, *54*, 6400; *Angew. Chem.* **2015**, *127*, 6498.
[12] a) S. Yamaguchi, S. Akiyama, K. Tamao, *J. Am. Chem. Soc.* **2001**, *123*, 11372; b) T. W. Hudnall, C.-. W. Chiu, F. P. Gabbaï, *Acc. Chem. Res.* **2009**, *42*, 388.
[13] a) C. R. Wade, A. E. J. Broomsgrove, S. Aldridge, F. Gabbaï, *Chem. Rev.* **2010**, *110*, 3985; b) F. Jäkle, *Chem. Rev.* **2010**, *110*, 3985; For selected reviews concerning applications in material chemistry see: c) A. Lorbach, A. Hübner, M. Wagner, *Dalton Trans.* **2012**, *41*, 6048; d) L. Ji, S. Griesbeck, T. B. Marder, *Chem. Sci.* **2017**, *8*, 846; e) M. Hirai, N. Tanaka, M. Sakai, S. Yamaguchi, *Chem. Rev.* **2019**, *119*, 8191.
[14] a) J. F. Blount, P. Finocchiaro, D. Gust, K. Mislow, *J. Am. Chem. Soc.* **1973**, *95*, 7019; b) K. Mislow, *Acc. Chem. Res.* **1976**, *9*, 26; c) D. Gust, K. Mislow, *J. Am. Chem. Soc.* **1973**, *95*, 1535; d) P. Finocchiaro, A. Recca, A. Bottino, F. Bickelhaupt, R. van Veen, H. Schenk, D. J. Schagen, *J. Am. Chem. Soc.* **1980**, *102*, 5594; e) J. P. Hummel, D. Gust, K. Mislow, *J. Am. Chem. Soc.* **1974**, *96*, 3679.
[15] K. Okada, H. Inokawa, M. Oda, *Tetrahedron Lett.* **1991**, *32*, 6363.
[16] H. Ito, T. Abe, K. Saigo, *Angew. Chem. Int. Ed.* **2011**, *50*, 7144; *Angew. Chem.* **2011**, *123*, 7282.
[17] a) M. Wang, C.-H. Zhao, *Chem. Rec.* **2022**, 22, e202100199; b) C. Wang, Z.-B. Sun, Q.-W. Xu, C.-H. Zhao, *Chem. Eur. J.* **2016**, *22*, 16750.
[18] a) M. Schnitzlein, K. Shoyama, F. Würthner, *Chem. Sci.* **2024**, *15*, 2984; b) K. Yuan, D. Volland, S. Kirschner, M. Uzelac, G. S. Nichol, A. Nowak-Król, M. J. Ingleson, *Chem. Sci.* **2022**, *13*, 1136; c) Y. Appiarius, S. Miguez-Lago, P. Puylaert, N. Wolf, S. Kumar, M. Molkenthin, D. Miguel, T. Neudecker, M. Jurıcek, A. G. Campañ, A. Staubitz, *Chem. Sci.* **2024**, *15*, 466. For other examples and recent reviews on bora- helicenes, see: d) A. Nowak-Król, P. T. Geppert, K. R. Naveen, *Chem. Sci.* **2024**, *15*, 7408; e) H.-W. Li, M. Li, Z.-H. Zhao, C.-F. Chen, Q. Peng, C.-H. Zhao, *Org. Lett.* **2021**, *23*, 4759; f) K. Dhbaibi, L. Favereau, J. Crassous, *Chem. Rev.* **2019**, *119*, 18846.
[19] a) A. Mazzanti, E. Mercanti, M. Mancinelli, *Org. Lett.* **2016**, *18*, 2692; b) A. Mazzanti, M. Boffa, E. Marotta, M. Mancinelli, *J. Org. Chem.* **2019**, *84*, 12253. For recent examples of C–B atropisomerism in boraza-heterocycles, see: c) K. Yang, Y. Mao, Z. Zhang, J. Xu, H. Wang, Y. He, P. Yu, Q. Song, *Nat. Commun.* **2023**, *14*, 4438; d) D. Pecorari, M. Mazzanti, S. Gianvittorio, S. Foschi, S. Stagni, V. Fiorini, M. Mancinelli, *Org. Chem. Front.* **2021**, *8*, 4496; e) K. Yang, Y. Mao, J. Xu, H. Wang, Y. He, W. Li, Q. Song, *J. Am. Chem. Soc.* **2021**, *143*, 10048; f) J. Wang, J.-W. Zhang, W. Bao, S.-Q. Qiu, S. Li, S.-H. Xiang, J. Song J Zhang, B. Tan, *J. Am. Chem. Soc.* **2021**, *143*, 12924.
[20] M. Birepinte, F. Robert, S. Pinet, L. Chabaud, M. Pucheault, *Org. Biomol. Chem.* **2020**, *18*, 3007.
[21] B. Kovács, T. Földes, M. Szabó, E. Dorkó, B. Kótai, G. Laczkó, T. Holczbauer, A. Domján, I. Pápai, T. Soós, *Chem. Sci.* **2024**, *15*, 15679.
[22] For recent reviews on chiral boron compounds, see: a) A.-M. Faisca-Phillips, A. J. L. Pombeiro, *Symmetry* **2024**, *16*, 11; b) A. Abdou-Mohamed, C. Aupic, C. Fournet, J.-L. Parrain, G. Chouraqui, O. Chuzel, *Chem. Soc. Rev.* **2023**, *52*, 4381.
[23] a) T.-H. Doan, A. Chardon, A. Osi, D. Mahaut, N. Tumanov, J. Wouters, B. Champagne, G. Berionni, *Chem. Eur. J.* **2021**, *27*, 1736; b) A. Chardon, A. Osi, D. Mahaut, T.-H. Doan, N. Tumanov, L. Fusaro, J. Wouters, B. Champagne, G. Berionni, *Angew. Chem. Int. Ed.* **2020**, *59*, 12402; *Angew. Chem.* **2020**, *132*, 12502; c) A. Ben Saida, A. Chardon, A. Osi, N. Tumanov, J. Wouters, A. I. Adjieufack, B. Champagne, G. Berionni, *Angew. Chem. Int. Ed.* **2019**, *58*, 16889; *Angew. Chem.* **2019**, *131*, 170; d) A. Osi, D. Mahaut, N. Tumanov, L. Fusaro, J. Wouters, B. Champagne, A. Chardon, G. Berionni, *Angew. Chem. Int. Ed.* **2022**, *61*, e202112342; *Angew. Chem.* **2022**, *134*, e202112342; e) A. Chardon, A. Osi, D. Mahaut, A. Ben Saida, G. Berionni, *Synlett* **2020**, *17*, 1639.
[24] a) A. Faulkner, T. van Leeuwen, B. L. Feringa, S. J. Wezenberg, *24.* **2016**, *138*, 13597; b) D. J. Qu, B. L. Feringa, *Angew. Chem. Int. Ed.* **2010**, *49*, 1107; *Angew. Chem.* **2010**, *122*, 1125; c) T. R. Kelly, M. C. Bowyer, K. V. Bhaskar, D. Bebbington, A. Garcia, F. Lang, M. H. Kim, M. P. Jette, *J. Am. Chem. Soc.* **1994**, *116*, 3657; d) S. J. Wezenberg, K.-Y. Chen, B. L. Feringa, *Angew. Chem. Int. Ed.* **2015**, *54*, 11457; *Angew. Chem.* **2015**, *127*, 11619.
[25] Deposition Number(s)2329754 (for **4b**), 2329755 (for **4e**), 2329756 (for **rac-4f**), 2329757 (for **4f-solution**), 2329758 (for **rac-4g**), 2329759 (for **4g-*R***), 2329760 (for **4g-*S***), 2329761 (for **rac-4i**), 2329762 (for **S17**), 2329763 (for **DTH2-161**), 2329764 (for **S9**), 2329765 (for **1h**), 2329766 (for **1i**), 2329767 (for **1k**), 2329768 (for **S14**), 2329769 (for **S16**) contain(s) the supplementary crystallographic data for this paper. These data are provided free of charge by the joint Cambridge Crystallographic Data Centre and Fachinformationszentrum Karlsruhe Access Structures service.
[26] M. Ōki, *Recent Advances in Atropisomerism, in Topics in Stereochemistry* (Eds.: E. L. Eliel, N. L. Allinger, S. H. Wilen) Wiley, **1983**; Vol. *14*, 1.
[27] J. Da Chai, M. Head-Gordon, *Phys. Chem. Chem. Phys.* **2008**, *10*, 6615.
[28] J. Da Chai, M. Head-Gordon, *J. Chem. Phys.* **2008**, *128*, 088106.
[29] B. Mennucci, R. Cammi, J. Tomasi, *Int. J. Quantum Chem.* **1999**, *75*, 767.

[30] J. Tomasi, B. Mennucci, R. Cammi, *Chem. Rev.* **2005**, *105*, 2999.
[31] M. J. Frisch, G. W. Trucks, H. B. Schlegel, G. E. Scuseria, M. A. Robb, J. R. Cheeseman, G. Scalmani, V. Barone, G. A. Petersson, H. Nakatsuji, X. Li, M. Caricato, A. V. Marenich, J. Bloino, B. G. Janesko, R. Gomperts, B. Mennucci, H. P. Hratchian, J. V. Ortiz, A. F. Izmaylov, J. L. Sonnenberg, D. Williams-Young, F. Ding, F. Lipparini, F. Egidi, J. Goings, B. Peng, A. Petrone, T. Henderson, D. Ranasinghe, V. G. Zakrzewski, J. Gao, N. Rega, G. Zheng, W. Liang, M. Hada, M. Ehara, K. Toyota, R. Fukuda, J. Hasegawa, M. Ishida, T. Nakajima, Y. Honda, O. Kitao, H. Nakai, T. Vreven, K. Throssell, J. A. Montgomery Jr., J. E. Peralta, F. Ogliaro, M. J. Bearpark, J. J. Heyd, E. N. Brothers, K. N. Kudin, V. N. Staroverov, T. A. Keith, R. Kobayashi, J. Normand, K. Raghavachari, A. P. Rendell, J. C. Burant, S. S. Iyengar, J. Tomasi, M. Cossi, J. M. Millam, M. Klene, C. Adamo, R. Cammi, J. W. Ochterski, R. L. Martin, K. Morokuma, O. Farkas, J. B. Foresman, D. J. Fox, Gaussian16 Revision A.03, (**2016**).
[32] A. Cnossen, J. C. M. Kistemaker, T. Kojima, B. L. Feringa, *J. Org. Chem.* **2014**, *79*, 927.

Manuscript received: November 11, 2024
Accepted manuscript online: February 19, 2025
Version of record online: ■■, ■■

Research Article

Atropisomerism

T.-H. Doan,* A. Chardon, N. Vanthuyne, T. N. Ramos, N. Tumanov, L. Fusaro, M. Albalat, L. Collard, J. Wouters, B. Champagne, G. Berionni* _____ e202421931

Atropisomerism in Triarylboranes: Lewis Base Assisted Rotation at C–B Stereogenic Axis in Asymmetrical Boron Lewis Acids

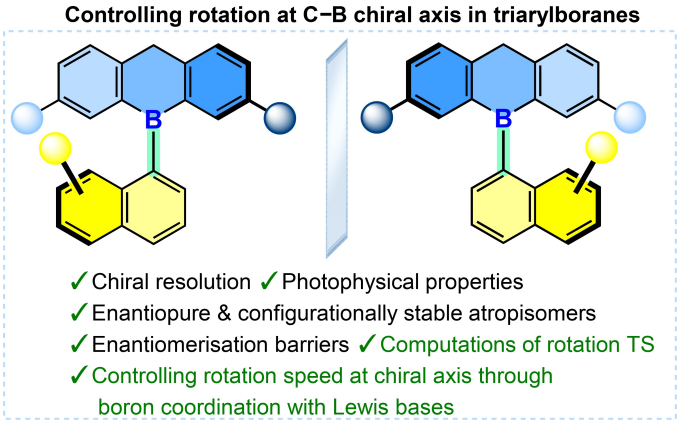

From decades to minutes: regulation of the rotation speed at the C–B chirality axis by *peri*-substituents and Lewis acid-base interactions in unprecedented triarylboranes with a C–B stereogenic axis enabled to reach atropostable and enantiopure triarylboranes.

Dr. Thu-Hong Doan
Dr. Aurélien Chardon
Dr. Nicolas Vanthuyne
Dr. Tárcius N. Ramos
Dr. Nikolay Tumanov
Dr. Luca Fusaro
Dr. Muriel Albalat
Laurent Collard
Prof. Johan Wouters
Prof. Benoît Champagne
Prof. Guillaume Berionni http://orcid.org/0000-0002-5422-9113

Author Contributions

Thu-Hong Doan: Conceptualization:Equal; Formal analysis:Lead; Methodology:Lead; Writing – original draft:Lead; Writing – review & editing:Equal
Aurélien Chardon: Investigation:Equal; Methodology:Equal; Resources:Equal; Visualization:Equal
Nicolas Vanthuyne: Data curation:Equal; Formal analysis:Equal
Tárcius N. Ramos: Data curation:Equal; Formal analysis:Equal
Nikolay Tumanov: Data curation:Equal; Formal analysis:Equal
Luca Fusaro: Data curation:Supporting; Formal analysis:Supporting
Muriel Albalat: Investigation:Equal; Methodology:Equal
Laurent Collard: Investigation:Equal; Methodology:Equal

Johan Wouters: Conceptualization:Equal; Funding acquisition:Equal; Supervision:Equal; Visualization: Equal
Benoît Champagne: Conceptualization:Equal; Funding acquisition:Equal; Software:Lead; Visualization: Equal
Guillaume Berionni: Conceptualization:Lead; Funding acquisition:Lead; Project administration:Lead; Resources:Lead; Supervision:Lead; Validation:Lead; Visualization:Equal; Writing – review & editing:Lead